electronic reprint

Journal of
**Synchrotron Radiation**
ISSN 0909-0495

# High-resolution wide-angle X-ray scattering of protein solutions: effect of beam dose on protein integrity

**Robert F. Fischetti, Diane J. Rodi, Ahmed Mirza, Thomas C. Irving, Elena Kondrashkina and Lee Makowski**

Copyright © International Union of Crystallography

Author(s) of this paper may load this reprint on their own web site provided that this cover page is retained. Republication of this article or its storage in electronic databases or the like is not permitted without prior permission in writing from the IUCr.

# High-resolution wide-angle X-ray scattering of protein solutions: effect of beam dose on protein integrity

**Robert F. Fischetti,[a,b] Diane J. Rodi,[b] Ahmed Mirza,[c] Thomas C. Irving,[d] Elena Kondrashkina[d] and Lee Makowski[b]***

*[a]GM/CA-CAT, Advanced Photon Source, Argonne National Laboratory, Argonne, IL 60439, USA, [b]Biosciences Division, Argonne National Laboratory, Argonne, IL 60439, USA, [c]Department of Biology, Illinois Institute of Technology, Chicago, IL 60616, USA, and [d]BioCAT, Advanced Photon Source, Argonne National Laboratory, Argonne, IL 60439, USA. E-mail: lmakowski@anl.gov*

Wide-angle X-ray scattering patterns from proteins in solution contain information relevant to the determination of protein fold. At relevant scattering angles, however, these data are weak, and the degree to which they might be used to categorize the fold of a protein is unknown. Preliminary work has been performed at the BioCAT insertion-device beamline at the Advanced Photon Source which demonstrates that one can collect X-ray scattering data from proteins in solution to spacings of at least 2.2 Å ($q$ = 2.8 Å$^{-1}$). These data are sensitive to protein conformational states, and are in good agreement with the scattering predicted by the program *CRYSOL* using the known three-dimensional atomic coordinates of the protein. An important issue in the exploitation of this technique as a tool for structural genomics is the extent to which the high intensity of X-rays available at third-generation synchrotron sources chemically or structurally damage proteins. Various data-collection protocols have been investigated demonstrating conditions under which structural degradation of even sensitive proteins can be minimized, making this technique a viable tool for protein fold categorization, the study of protein folding, unfolding, protein–ligand interactions and domain movement.

**Keywords: wide-angle X-ray scattering; diffraction; protein structure; radiation damage; third-generation synchrotron sources.**

## 1. Introduction

Small-angle X-ray scattering (SAXS) from biological macromolecules in solution is a technique that yields information on the overall shape of the molecule, and can monitor conformational changes, including molecular associations in solution (for review see Trewella, 1997). Although wide-angle scattering has the potential to provide higher-resolution structural information, practical use of the data has been limited by the difficulty of measuring the weak protein scattering which is superimposed on a much stronger background of scatter from the solvent and sample container. Recently, it has been demonstrated that wide-angle scattering patterns (WAXS) obtained on insertion-device beamlines at third-generation synchrotron sources are not only sensitive to protein conformation states, but also that the scattering patterns generated can be quantitatively compared with data calculated from detailed structural models (Svergun *et al.*, 1995; Hirai *et al.*, 2002). These data provide a rich source of structural information that has not yet been exploited. A combination of SAXS and WAXS analysis has the potential to generate information on the size, shape and structural class (*i.e.* fold) of the large fraction of proteins that may not form crystals. It is applicable to all classes of proteins including membrane proteins, large protein complexes and proteins with disordered regions. An unambiguous determination of fold cannot be obtained directly from solution scattering data (Svergun *et al.*, 2001), but a comparison of solution scattering from proteins of unknown structure with data from proteins of known structure has the potential to reduce the number of possible folds for a protein to a short list, if not a unique designation.

A potential obstacle to obtaining structural information by WAXS is radiation-induced damage to the protein structure from the intense X-ray beam on undulator source beamlines. This has been shown to be a significant problem in protein X-ray crystallography (*e.g.* Ravelli & McSweeney, 2000). Radiation exposure can induce chemical and structural damage to protein crystals such as cleavage of disulfide bonds, decarboxylation of acidic residues, and an increase in both atomic $B$-factors and unit-cell volume (Helliwell, 1988; Burmeister, 2000; Ravelli & McSweeney, 2000; Teng & Moffat, 2000; Weik *et al.*, 2000). Data recorded from trypsin crystals on different bending-magnet and insertion-device beamlines at the ESRF showed an increased rate of decay (Leiros *et al.*, 2001). However, from these observations one could not determine if the increased rate of damage was in proportion to the total dose or the dose rate. The use of crystals at liquid-nitrogen temperatures has greatly alleviated the problem of radiation damage in crystallography and a similar approach may be adaptable for WAXS. It is anticipated, however, that this approach would lead to serious problems in background scaling and subtraction due to the increased scattering from the ice crystals, and thus limit the use of WAXS for dynamic studies. We approach the problem by using a sample flow cell that minimizes the radiation dose to individual proteins and show that this approach eliminates observable changes in scattering due to radiation damage.

Here we demonstrate the capability of collecting X-ray scattering data from proteins in solution to spacings of 2.2 Å (or $q$ = 2.8 Å$^{-1}$), show that these data are consistent with expectations based on known crystallographic coordinates, show that these data are sensitive indicators of conformational changes of a protein in solution, demonstrate the use of WAXS as a monitor of the effect of chemical denaturing conditions on proteins, and show that the effect of radiation damage can be observed and evaluated using this method.

## 2. Methods

### 2.1. Materials

Equine heart cytochrome C from Sigma (molecular weight 12.4 kDa) and equine skeletal muscle myoglobin (molecular weight 17.8 kDa) from Sigma were dissolved in sterile deionized water to 30 mg ml$^{-1}$ and 20 mg ml$^{-1}$, respectively. Bovine erythrocyte hemoglobin (molecular weight 64.5 kDa) from CalBiochem was dissolved in sterile PBS (phosphate-buffered saline; 137 m$M$ NaCl, 2.7 m$M$ KCl, 10 m$M$ $Na_2HPO_4$, 2 m$M$ $KH_2PO_4$) from Biowhittaker to 60 mg ml$^{-1}$. Protein samples were centrifuged through a Nanosep centrifugal device (molecular weight cut-off = 300 kDa; Pall Corporation) for 10 min prior to beam exposure to remove high-molecular-weight protein aggregates from solution. Protein solutions were denatured by adding crystalline guanidine hydrochloride (Pierce Chemical).

### 2.2. X-ray scattering data

Wide-angle X-ray scattering (WAXS) data were collected at the BioCAT undulator beamline (18ID) at the Advanced Photon Source (APS), Argonne, IL, USA (Irving *et al.*, 2000). The experimental layout was arranged as follows. A nitrogen-gas-filled ion chamber was

 © 2003 International Union of Crystallography • Printed in Great Britain – all rights reserved 

electronic reprint

used to record the X-ray beam intensity. In-vacuum guard slits were set to remove low-angle scatter from the X-ray optics and upstream windows. Another set of guard slits was positioned about 4 mm in front of the sample to remove scatter from the vacuum exit window (mica) and small air gap. The sample cell consisted of a thin-walled quartz capillary (1 mm inner diameter) attached to a programmable pump (Hamilton Microlab 500 series) that could be adjusted to deliver either continuous or discontinuous flow through the capillary. A helium-gas-filled path with a mica entrance window and a 0.5 mm mylar exit window was positioned between the capillary and the detector. Scattering from the mylar exit window was blocked by positioning the beam stop to touch the mylar window. The X-ray scattering pattern was detected with a CCD detector specially designed for imaging measurements requiring high sensitivity (a dynamic range of 10000 to 1) and high spatial resolution (48 μm × 48 μm; 1798 × 1028 pixels) (Phillips *et al.*, 2002). The specimen-to-detector distance was 148 mm.

The X-ray beam was focused to 40 μm × 180 μm (vertical × horizontal, FWHM) at the detector. Owing to the long depth of focus, the beam was only slightly larger at the specimen. The beamline is capable of delivering approximately $2 \times 10^{13}$ photons $s^{-1}$ per 100 mA of beam current. Previous experience on the BioCAT beamline, however, has demonstrated that proteins under a variety of physical conditions are damaged after exposure times of a few tenths of a second to a few seconds at these intensity levels. In these experiments, thin aluminium foils were used as X-ray beam attenuators to control the incident beam flux.

The two-dimensional scattering patterns were integrated radially to one-dimensional scattering intensity profiles using the program *Fit2D*, version 9.129 (Hammersley, 1997, 1998; Hammersley *et al.*, 1996). The origin of the diffraction pattern was determined by calculating the center of powder diffraction rings from silver behenate powder. The incident X-ray beam intensity was recorded and used to normalize the individual exposures.

In order to assess the effect of radiation dose on proteins, three scattering data-collection modes were employed:

(i) Data collected as a series of 0.7 s exposures from protein samples sitting stationary within the sample cell in the beam path (ST or stationary mode);

(ii) Data collected as a series of 8.3 s exposures from protein samples that were oscillated within the sample capillary at a rate of 10.3 oscillations $min^{-1}$ during beam exposure (FR or fry mode);

(iii) Data collected as a series of 8.3 s exposures from protein samples that were kept flowing unidirectionally through the beam during exposure, so that no one part of the solution was exposed more than once in the direct beam (RD or reduced-exposure mode). The flow rate was adjusted so that no single section of the protein column spent more than 100 ms in the direct beam (2.4 μL $s^{-1}$).

Data were also collected from the empty sample capillary and from the capillary containing buffer. Exposures from sample and buffer were alternated to minimize the possible effects of drift in any experimental parameter.

### 2.3. Estimation of diffraction from protein

Scattering from samples should be separable into four individual components: that owing to scattering from the protein; from the bulk solvent; from the solvent of hydration; and from the capillary. Scattering from the solvent of hydration (boundary layer), although potentially important at small angles of scattering, is generally at least two orders of magnitude weaker than any other contribution in the range of angles studied here (Svergun *et al.*, 1995). Scattering from protein was estimated according to

$$I_{\rm prot} = I_{\rm obs} - I_{\rm cap} - (1 - {\rm vol}\%) I_{\rm solvent}, \quad (1)$$

where $I_{\rm obs}$ was the measured scattering from the protein sample; $I_{\rm cap}$ the measured scattering from the empty capillary; vol% the estimated proportion of the solution taken up by the protein (and thereby excluding solvent), and $I_{\rm solvent}$ was estimated by

$$I_{\rm solvent} = I_{\rm bkgd} - I_{\rm cap}, \quad (2)$$

where $I_{\rm bkgd}$ is the measured scattering from the capillary containing buffer. The volume percent of the cytochrome C sample was approximately 2.5% (30 mg $ml^{-1}$), and based on that estimate the intensity of diffraction from the protein was calculated. Scaling was based on the total dose estimated as described above. Small ambiguities (less than one-tenth of 1%) in the relative scaling of the scattering from solvent, capillary and protein solution lead to some uncertainty in the scaling of higher-angle features relative to the features in the 0.1 $Å^{-1}$ range. These were resolved on the basis of self-consistency of features in patterns from homologous proteins.

### 2.4. Prediction of scatter from protein

WAXS patterns were calculated from crystallographic coordinates using the program *CRYSOL* (version 2.3, http://www.embl-hamburg.de/ExternalInfo/Research/Sax/manual_crysol.html) using 50 spherical harmonics and default parameters for calculation of solvation shell and particle envelope. A maximum allowed number of Fibonacci grid points of 18 was used for all calculations. No attempt was made to directly fit the *CRYSOL*-calculated pattern to the experimental data.

### 2.5. Analysis of samples

SDS polyacrylamide gel electrophoresis of protein samples pre- and post-beam exposure was carried out as per a modified version of Laemmli (Laemmli, 1970). Briefly, aliquots of protein samples were diluted in protein dilution buffer (100 m*M* $KHPO_4$, pH 7.2, 100 m*M* NaCl, 10% *v*/*v* glycerol, 0.02% $NaN_3$), mixed 1:1 *v*/*v* with 2X Laemmli sample buffer minus reducing agent (Sigma), heated to 368 K for 10 min, cooled on ice, then loaded onto a 5% stacking/12% resolving SDS polyacrylamide gel. Samples were run at a constant 10 V $cm^{-1}$ alongside low-range molecular-weight protein markers (BioRad). The gel was stained with Simply Blue Safe Stain (Invitrogen) for 1 h, followed by extensive destaining over 10 h in multiple changes of deionized water.

## 3. Results and discussion

### 3.1. Effect of data-collection strategy on measurable radiation damage

A major concern in the use of third-generation sources is radiation damage to proteins because of the available high intensities (see above references). Most crystallographic stations use crystals flash-frozen in the presence of cryoprotectants to minimize the effect of radiation on protein structure. The experiments described here were carried out at room temperature and heating due to X-ray exposure was not monitored. Initial data-collection protocols were designed to assess the effect of radiation damage under these conditions. Background diffraction was subtracted from each protein solution scattering pattern using equation (1). Background-subtracted scattering profiles for hemoglobin in all three beam exposure modes (*i.e.* RD, FR and ST mode-generated profiles) were calculated and contrasted.



electronic reprint

The patterns for hemoglobin demonstrated significant deviations between the RD and FR modes (virtually identical) and the ST mode. Fig. 1 shows the average from ten ST shots (10 × 0.5 s = 5 s total exposure) in black contrasted with the average of four RD shots (8.1 s × 4 = 32.4 s total exposure) in red. The protein sample in the stationary (ST) mode shows clear signs of degradation across the entire pattern, indicating a breakdown of features within the size range for both secondary and tertiary structure (note the partial loss of peaks at spacings of roughly 0.08 and 0.095 Å and filling in of minima). The different noise levels apparent in the two plots are the result of different total exposure times, not radiation damage.

A plot of serially measured scattering curves in ST mode from a single hemoglobin solution (Fig. 2*a*) demonstrates this point more clearly. As each data set is taken, a progressive flattening of peak intensity (black curve to blue to green to red) can be seen (follow arrow). These differences can also be seen by looking at a comparison of the first data set measured (black curve, Fig. 2*b*) and the tenth data set measured (red curve, Fig. 2*b*). Significant curve flattening can be seen at spacings consistent with quaternary structure (black arrow), tertiary structure (red arrow) and secondary structure (green arrow), demonstrating an overall breakdown of structure. Scattering profiles in RD and FR modes demonstrated no detectable progressive degradation patterns (data not shown). A third set of scattering measurements obtained from hemoglobin in ST mode but with an increased number of foils to reduce the beam flux (from 28 or 10.3-fold attenuation to 32 or 13.8-fold attenuation) similarly showed no detectable progressive structure degradation.

In Fig. 3, analogous data for myoglobin in RD mode (red) is compared with data collected using 0.7 s exposures to a stationary sample (ST mode; black; shown is the average of ten 0.7 s exposures). The two data sets are identical to within the counting errors. Note that the signal-to-noise ratio is much lower for the ST mode because the data shown corresponds to a total exposure of about 0.7 s × 8 = 5.6 s or only about 15% of that used for data collected in RD mode (8.3 s × 5 or 41.5 s).

None of the samples were moved between exposures during the series of still shots (ST mode). Nevertheless, no progressive degradation was observed within the myoglobin or cytochrome C series (data not shown) and data from the first and last exposures were identical to within counting statistics. Given the sensitivity of hemoglobin to repeated beam flux exposure as shown in Figs. 1 and 2, data obtained with that protein were used as an indicator of maximal sensitivity, and all further work was performed in RD mode with 28 attenuator foils (10.3-fold flux attenuation) to obtain maximal signal intensity while minimizing protein structure breakdown.

Denaturing gel electrophoresis of aliquots from all three protein samples pre- and post-beam exposure was carried out to determine whether any chemical degradation occurred as a result of X-ray exposure. Non-reducing SDS gel electrophoresis revealed no detectable crosslinking or cleavage reactions occurring upon irradiation (see Fig. 4). No new bands of either higher or lower molecular weight were seen following irradiation (Fig. 4, lanes *c*, *e* and *g*), even in grossly overloaded lanes (Fig. 4, lanes *c* and *e*), and no detectable

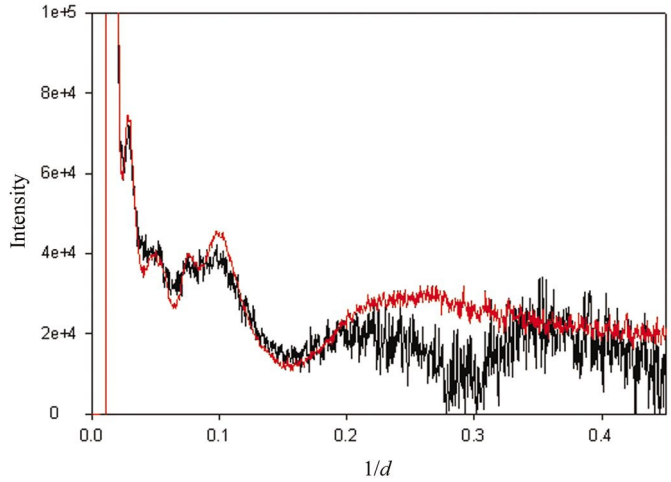


**Figure 1**
Comparison of the average solution scattering profiles obtained from hemoglobin using RD data-collection mode (red) and ST data-collection mode (black). Note that the ST mode shows clear signs of degradation. The abscissa is in arbitrary units for relative intensity, and the ordinate is in units of Å$^{-1}$.

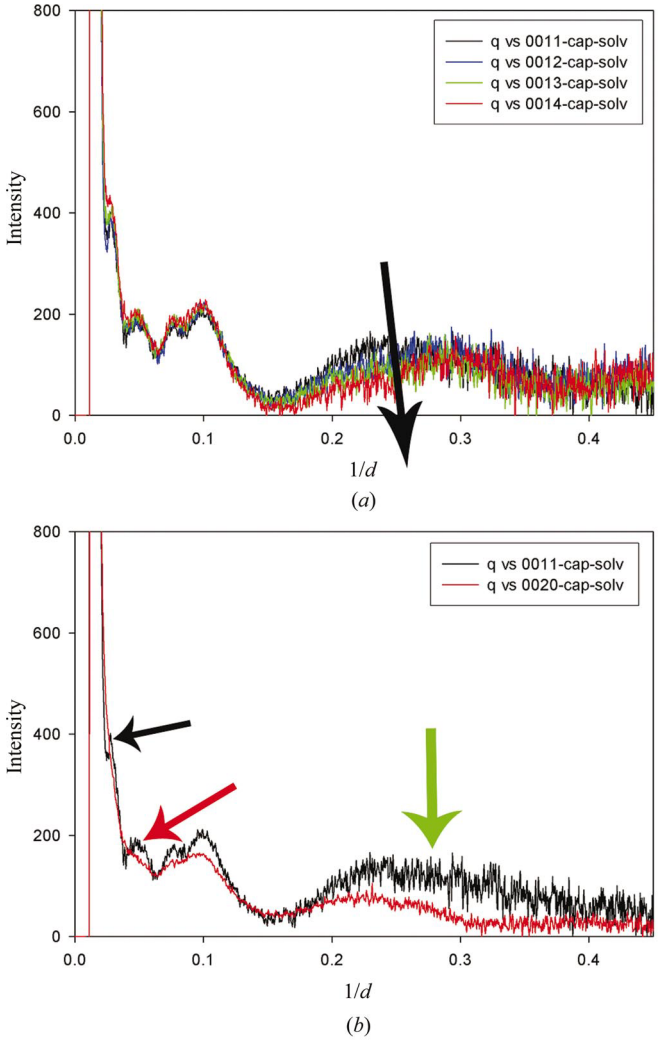


**Figure 2**
Wide-angle scattering curves from hemoglobin using ST data-collection mode. (*a*) This curve set is a series of measured scattering profiles from a single stationary protein solution, in the exposure order of black/blue/green/red. Note that the trend as the X-ray exposure increased is progressive structure degradation as evidenced by the overall flattening of the curve. (*b*) Isolation of the first and tenth data sets (black and red, respectively) demonstrates the eventual loss of the quaternary structure-associated peak (black arrow) and a tertiary structure associated peak (red arrow), plus an overall flattening in the secondary structure region spacing (green arrow). The abscissa is in arbitrary units for relative intensity, and the ordinate is in units of Å$^{-1}$.


electronic reprint

disulfide bond cleavage of globin homodimers was observed (Fig. 4, lanes *g* and *f*), as the ratio of dimer to monomer remained roughly unchanged. These data imply that the only X-ray beam induced damage detectable at this level of analysis was at the secondary and tertiary structure level.

### 3.2. Comparison of calculated and observed diffraction

Background diffraction was subtracted from each protein solution scattering pattern using equation (1), then compared with the diffraction pattern calculated from atomic coordinates [PDB files 1CRC (using only chain A) for cytochrome C, 1WLA for myoglobin and 1GZX for hemoglobin] using the most recent version of the program *CRYSOL* (Svergun *et al.*, 1995). The correspondence of calculated and observed diffraction for cytochrome C, shown in Fig. 5, indicated that the measured scattering from the protein, although low compared with background scatter, was consistent with expectations based on the atomic coordinates of cytochrome C ($R$-factor = 0.125). There is good agreement in both peak position and relative heights for both plots. A somewhat lower degree of correspondence was obtained for both myoglobin (Fig. 6) and hemoglobin (Fig. 7), with $R$-factors of 0.21 and 0.23, respectively.

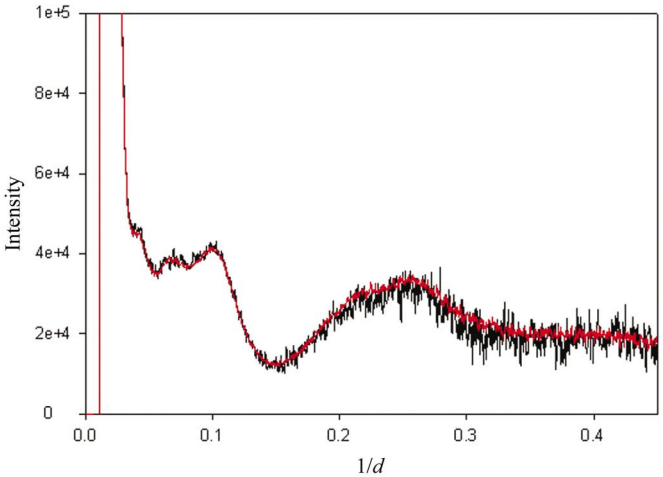


**Figure 3**
Comparison of the average solution scattering profiles obtained from myoglobin using RD data-collection mode (red) and ST data-collection mode (black). The abscissa is in arbitrary units for relative intensity, and the ordinate is in units of Å$^{-1}$.

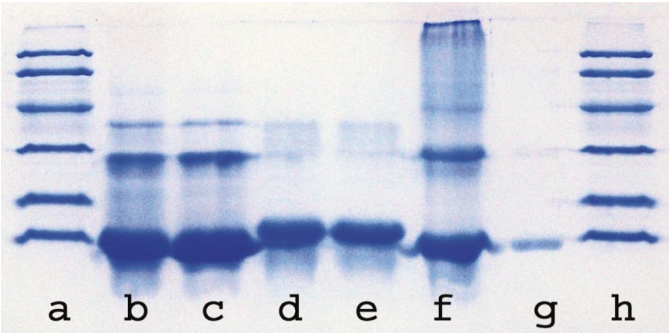


**Figure 4**
Non-reducing SDS polyacrylamide gel of unexposed and exposed cytochrome C (lanes *b* and *c*), myoglobin (lanes *d* and *e*), and hemoglobin (lanes *f* and *g*). Lanes *a* and *h* are duplicate loadings of standard proteins of molecular weight (in descending order from top to bottom): 112, 81, 49.9, 36.2, 29.9 and 21.3 kDa.

The differences seen between the measured and calculated diffraction could arise from either experimental error or actual structural differences between the protein in a crystal and in solution. The most likely source of experimental error would be small errors in the scaling of the observed scatter from protein solution, buffer and capillary. This could lead to errors in base line and in the overall distribution of intensity across the pattern. Errors of this kind, however, do not result in artifactual high-frequency details. The degree to which the derived experimental scatter from protein depends on these scale factors was explored extensively and no combination of parameters resulted in a significantly closer correspondence between calculated and observed scatter (data not shown).

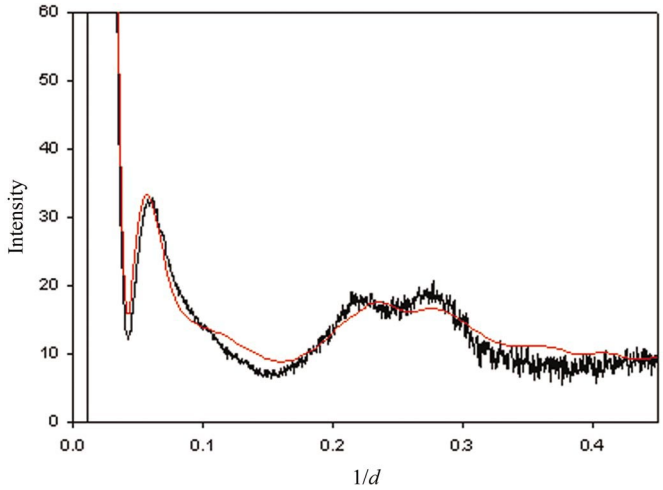


**Figure 5**
Wide-angle scattering curves for cytochrome C. The black curve is the theoretical solution scattering curve calculated using *CRYSOL* with 50 spherical harmonics as described in §2. The red curve is the measured scattering solution curve obtained with data-collection mode RD as described in §2. The abscissa is in arbitrary units for relative intensity, and the ordinate is in units of Å$^{-1}$.

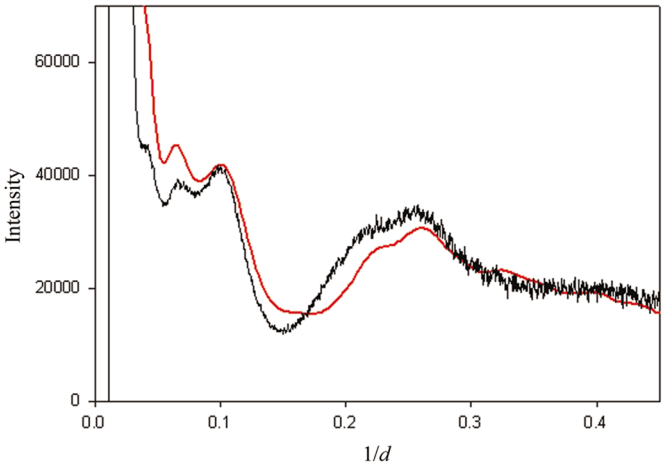


**Figure 6**
Wide-angle scattering curves for myoglobin. The red curve is the theoretical solution scattering curve calculated using *CRYSOL* with 50 spherical harmonics as described in §2. The black curve is the measured scattering solution curve obtained with data-collection mode RD as described in §2. The abscissa is in arbitrary units for relative intensity, and the ordinate is in units of Å$^{-1}$.



electronic reprint

An obvious source of disparity between the measured and calculated scattering profiles is that the calculated patterns were derived from atomic coordinates from X-ray crystallographic data. The incorporation of the proteins into a crystalline lattice may result in changes either to the average structure or to the degree of flexibility of the molecule. These changes, where they occur, would contribute to the differences observed between calculated and measured scatter profiles. Differences observed between scattering- and crystal-derived structural features (Heidorn & Trewhella, 1988; Hubbard *et al.*, 1988; Timchenko *et al.*, 2000) have provided valuable information regarding domain–domain movements and macromolecular ring sizes. For example, Fig. 7 shows that for hemoglobin there is a calculated peak centered at 0.11 Å$^{-1}$ that corresponds to the observed peak at 0.10 Å$^{-1}$. This shift could reflect a loosening of the structure in solution as compared with in the crystal.

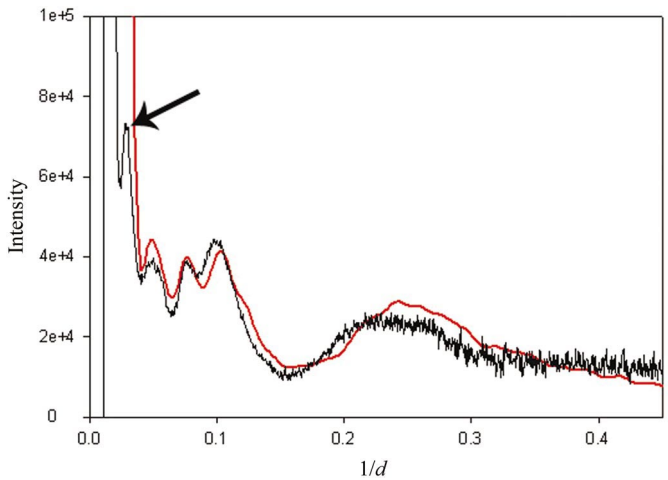


**Figure 7**
Wide-angle scattering curves for hemoglobin. The red curve is the theoretical solution scattering curve calculated using *CRYSOL* with 50 spherical harmonics as described in §2. The black curve is the measured scattering solution curve obtained with data-collection mode RD as described in §2. The abscissa is in arbitrary units for relative intensity, and the ordinate is in units of Å$^{-1}$.

### 3.3. Comparative structural analysis

Comparison of diffraction from the structurally related proteins myoglobin and hemoglobin in Fig. 8 provides additional insight into the kind of information that can be obtained from solution scattering data. Hemoglobin is a tetramer of four polypeptides, each of which exhibits a fold very similar to that of myoglobin. This quaternary structure of hemoglobin results in a higher-frequency modulation of data out to a spacing of about 0.15 Å$^{-1}$. In particular, note the presence of an additional peak in the hemoglobin scattering at about 0.031 Å$^{-1}$ (see black arrows in Figs. 7 and 8). At spacings higher than 0.15 Å$^{-1}$ the data from the two proteins are very similar, reflecting their very similar secondary structures. Although the secondary structure of a protein also contributes to the scattering at intermediate spacings (0.05–0.15 Å$^{-1}$), this is modulated by the effect of both tertiary and quaternary structure.

### 3.4. Effect of chemical denaturants

To explore the use of WAXS for the study of protein unfolding, hemoglobin samples were intentionally denatured by the addition of crystalline guanidine hydrochloride to 2 molar and then 4 molar final concentrations, and then exposed to the beam in RD mode (Fig. 9). On addition of guanidine-HCl to 2*M* there is a significant loss of features at both high spacings (over 0.3 Å$^{-1}$) and lower spacings (see red curve in Fig. 9). Note that there is a complete loss of the tetrameric form-associated peak at 0.029 to 0.030 Å$^{-1}$ spacing. Further addition of guanidine-HCl to 4*M* shows a catastrophic loss of structure over the entire pattern (blue curve in Fig. 9). A comparison of Figs. 2 and 9 shows that treatment of hemoglobin with both 2*M* guanidine-HCl and ST mode data collection both result in the loss of the tertiary structure-related doublet at spacings of about 0.1 Å$^{-1}$ and the peak at 0.031 Å$^{-1}$ associated with the presence of the tetrameric structure. These data infer that, in spite of different

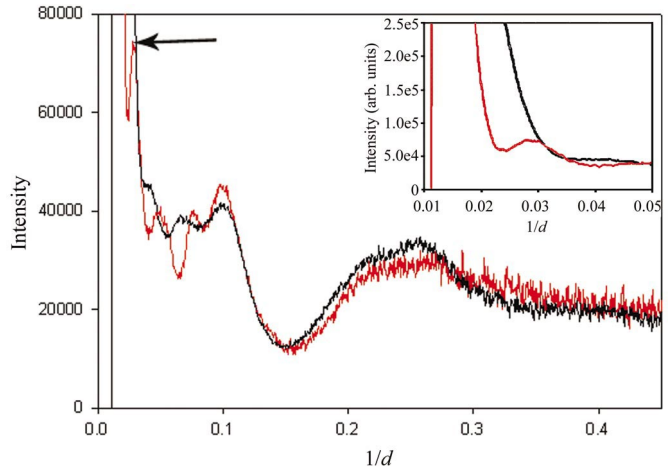


**Figure 8**
Comparison of measured solution scattering curves for the related proteins myoglobin and hemoglobin. The black curve is myoglobin, the red curve is hemoglobin. Note that the quaternary structure of hemoglobin as compared with the monomeric myoglobin leads to additional high-frequency fluctuations in the 1/*d* range 0.021–0.09 Å$^{-1}$. The abscissa is in arbitrary units for relative intensity, and the ordinate is in units of Å$^{-1}$. Detail of the peak at 0.03 Å$^{-1}$ in the scattering from hemoglobin is shown in the inset contrasted with the myoglobin scattering curve devoid of that peak.

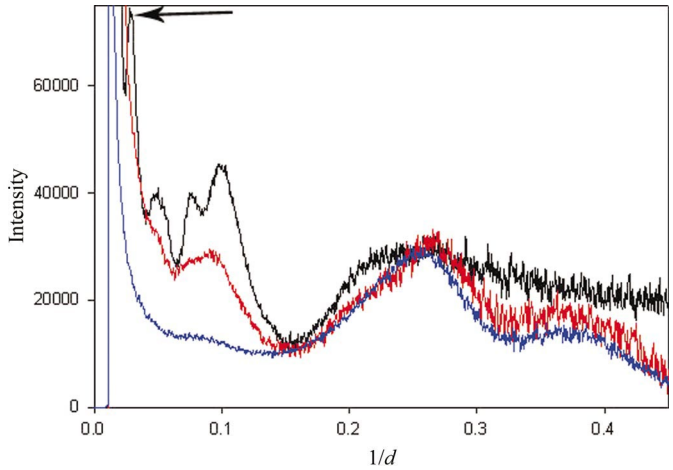


**Figure 9**
Effect of increasing concentration of guanidine hydrochloride on the solution scattering profile from hemoglobin. The black curve is 0*M* guanidine hydrochloride, the red curve is 2*M* guanidine hydrochloride and the blue curve is 4*M* guanidine hydrochloride. Note that the addition of guanidine hydrochloride to 2*M* completely obliterates the peak at 1/*d* of around 0.029 Å$^{-1}$, a spacing which is consistent with the tetrameric form of hemoglobin. The abscissa is in arbitrary units for relative intensity, and the ordinate is in units of Å$^{-1}$.


electronic reprint

mechanisms of action, both chemical denaturants and radiation result in the dissociation of the hemoglobin tetramer, similar to the oligomeric shifting effect seen in a study of yeast pyruvate decarboxylase (Konig *et al.*, 1992). Guinier plots of the small-angle X-ray scattering data from hemoglobin in 0*M*, 2*M* and 4*M* guanidine-HCl indicate radii of gyration consistent with tetrameric, dimeric and monomeric structures, respectively. At 0*M* guanidine-HCl the observed radius of gyration was 25.7 Å, which is within 3% of the 26.4 Å calculated for a tetramer from crystallographic coordinates. For 2*M* guanidine-HCl the observed radius of gyration was 23.0 Å or within 13% of that calculated for an $\alpha\beta$-dimer (20.3 Å). For 4*M* guanidine-HCl the observed radius of gyration was approximately 50 Å, corresponding to unfolded monomers.

Identical treatment of myoglobin with 2*M* and 4*M* guanidine-HCl resulted in a pattern of degradation similar to that of hemoglobin but less pronounced, suggesting that myoglobin is more resistant than hemoglobin to the effect of guanidine-HCl (Fig. 10). A similar differential sensitivity is observed with increasing radiation dose (see Fig. 1 *versus* Fig. 3). Previous work has shown that exposure of hemoglobin and myoglobin to $^{\bullet}$OH radicals in the presence of oxygen causes a similar level of fragmentation product formation (Davies, 1987). Intentional denaturation of holomyoglobin with a number of agents demonstrated that the stability of the protein is almost exclusively determined by heme affinity, not the folding properties of the apoprotein (Hargrove & Olson, 1996). Myoglobin has a much higher affinity for hemin than hemoglobin, whereas hemoglobin's hemin affinity is regulated by its quaternary structure (*i.e.* enhanced) (Hargrove *et al.*, 1997). The most likely scenario during beam exposure is that oxygen radical-induced oxidation of the three cysteines in hemoglobin cause the tetramer to dissociate (as can be seen in the loss of the quaternary structure-associated scattering peak). As the dimers and monomers autooxidize and lose hemin much more rapidly than the tetramers, the process of complete denaturation is accelerated for hemoglobin. Myoglobin, by contrast, has no thiols and would be expected to exhibit higher stability to X-ray-generated radicals. A reason for differential sensitivity to guanidine HCl denaturation is less obvious. The patterns of side-chain contacts are clearly different between the two proteins. The higher-order structure, cooperativity and structural switch of hemoglobin may demand a less rigid and less resilient set of stabilizing interactions. It is possible that the breakdown of the hemoglobin tetramer, whether by denaturant or by radiation, exposes hydrophobic surfaces which, on exposure to solvent, accelerates structure degradation.

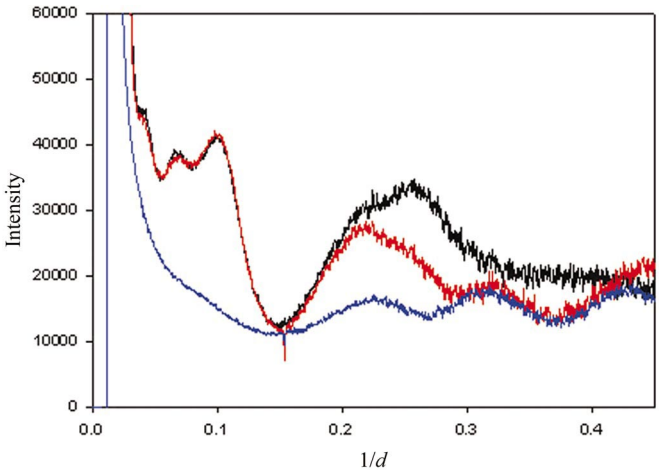


**Figure 10**
Effect of increasing concentration of guanidine hydrochloride on the solution scattering profile from myoglobin. The black curve is 0*M* guanidine hydrochloride, the red curve is 2*M* guanidine hydrochloride and the blue curve is 4*M* guanidine hydrochloride. Note that the addition of guanidine hydrochloride to 2*M* has almost no effect in the tertiary structure region (0.05–0.14 Å$^{-1}$), yet flattens the scattering curve in the secondary structure region at higher 1/*d* values. The abscissa is in arbitrary units for relative intensity, and the ordinate is in units of Å$^{-1}$.

## 4. Conclusions

It is becoming increasingly apparent that three-dimensional structural information will be critical in making a comprehensive functional analysis of many, if not most, proteins. For the majority of proteins that cannot be readily crystallized, new methods of structural characterization are needed. For those proteins that can be crystallized, methods for characterization of functional processes that are accompanied by large structural changes will be required. X-ray scattering from proteins in solution provides direct structural information about the secondary, tertiary and quaternary organization of a protein. With optimized hardware and software, this data can be collected in a high-throughput fashion to provide information about three-dimensional structures and structural changes that occur in solution.

A major concern for X-ray scattering of protein solutions is radiation-induced degradation by the high intensities available at the third-generation synchrotron radiation source utilized in these studies. Earlier work performed at the JASRI at SPring-8 (Hirai *et al.*, 2002) involving 60 s exposure times to collect data at spacings of ~0.003–0.4 Å$^{-1}$ did not specifically address the issue of protein degradation at third-generation sources. This may be a function of their use of a bending-magnet beamline and a large flat cell, both of which would be anticipated to lower radiation-induced damage to the protein molecules. The data presented here indicate that, while X-ray damage is observable when proteins are intentionally overexposed to X-rays using an insertion-device beamline, experimental protocols can be designed to minimize that damage while maximizing the signal intensity obtained.

These solution scattering experiments on cytochrome C, myoglobin and hemoglobin indicate that accurate solution scattering data can be collected to spacings approaching 2.2 Å; that this data can be adequately predicted from the atomic coordinates of crystallized proteins; that it can be used for comparative structural analyses; and that it can monitor structural changes that occur in the sample. Unlike circular dichroism (CD) spectroscopy, which provides extensive short-range information on the percentage content of $\alpha$-helices, $\beta$-sheets *etc.*, the data shown here demonstrate a sensitivity to tertiary and quaternary structural influences that are not apparent in CD spectra. This suggests that WAXS may ultimately prove to be a valuable tool for the rapid confirmation or rejection of structural hypotheses derived from amino acid sequence data *via* bioinformatic analysis. The impact of WAXS data would grow substantially if an extensive database of solution scattering from proteins of known structure were constructed. This database could provide the basis for making predictions about the domain and fold structure of proteins of unknown structure and make possible detailed structural analyses of dynamic functional processes.

The authors would like to thank Dmitri I. Svergun, Fred Stevens, Gerd Rosenbaum and Rose Wilton for helpful discussions, and the staff and scientists of Sector 18 at the APS for use of the facilities. Access to additional data and primary image files can be gained *via*



electronic reprint

the web link http://biotopia.bio.anl.gov/drodi/index.html under 'Scattering project'. Use of the Advanced Photon Source was supported by the US Department of Energy, Basic Energy Sciences, Office of Science, under contract No. W-31-109-ENG-38. BioCAT is a National Institutes of Health-supported Research Center RR-08630.

### References

Burmeister, W. P. (2000). *Acta Cryst.* D**56**, 328–341.
Davies, K. J. A. (1987). *J. Biol. Chem.* **262**, 9895–9901.
Hammersley, A. P. (1997). ESRF Internal Report ESRF97HA02T. ESRF, Grenoble, France.
Hammersley, A. P. (1998). ESRF Internal Report ESRF98HA01T. ESRF, Grenoble, France.
Hammersley, A. P., Svensson, S. O., Hanfland, M., Fitch, A. N. & Häusermann, D. (1996). *High Press. Res.* **14**, 235–248.
Hargrove, M. S. & Olson, J. S. (1996). *Biochemistry*, **35**, 11 310–11 318.
Hargrove, M. S., Whitaker, T., Olson, J. S., Vali, R. J. & Mathews, A. J. (1997). *J. Biol. Chem.* **272**, 17385–17389.
Heidorn, D. B. & Trewhella, J. (1988). *Biochemistry*, **27**, 909–915.
Helliwell, J. R. (1988). *J. Cryst. Growth*, **90**, 259–272.
Hirai, M., Iwase, H., Hayakawa, T., Miura, K. & Inoue, K. (2002). *J. Synchrotron Rad.* **9**, 202–205.
Hubbard, S. R., Hodgson, K. O. & Doniach, S. (1988). *J. Biol. Chem.* **263**, 4151–4158.
Irving, T. C., Fischetti, R., Rosenbaum, G. & Bunker, G. B. (2000). *Nucl. Instrum. Methods A*, **448**, 250–254.
Konig, S., Svergun, D., Koch, M. H., Hubner, G. & Schellenberger, A. (1992). *Biochemistry*, **37**, 8726–8731.
Laemmli, U. K. (1970). *Nature (London)*, **227**, 680–685.
Leiros, H.-K. S., McSweeney, S. M. & Smalås, A. O. (2001). *Acta Cryst.* D**57**, 488–497.
Phillips, W. C., Stewart, A., Stanton, M., Naday, I. & Ingersoll, C. (2002). *J. Synchrotron Rad.* **9**, 36–43.
Ravelli, R. B. & McSweeney, S. M. (2000). *Struct. Fold. Des.* **8**, 315–328.
Svergun, D., Barferato, C. & Koch, M. H. J. (1995). *J. Appl. Cryst.* **28**, 768–773.
Svergun, D. I., Petoukhov, M. V. & Koch, M. H. (2001). *Biophys. J.* **80**, 2946–2953.
Teng, T.-Y. & Moffat, K. (2000). *J. Synchrotron Rad.* **7**, 313–317.
Timchenko, A. A., Melnik, B. S., Kihara, H., Kimura, K. & Semisotnov, G. V. (2000). *FEBS Lett.* **471**, 211–214.
Trewella, J. (1997). *Curr. Opin. Struct. Biol.* **7**, 702–708.
Weik, M., Ravelli, R. B., Kryger, G., McSweeney, S., Raves, M. L., Harel, M., Gros, P., Silman, I., Kroon, J. & Sussman, J. L. (2000). *Proc. Natl. Acad. Sci. USA*, **97**, 623–628.

 Received 25 April 2003 • Accepted 29 July 2003 

electronic reprint